IEEE Access
Multidisciplinary | Rapid Review | Open Access Journal

Received 25 October 2021, accepted 31 December 2021, date of publication 18 January 2022, date of current version 7 September 2022.

Digital Object Identifier 10.1109/ACCESS.2022.3144248

An Optimal Energy Absorption and Utilization Design for Deformable/Reconfigurable Modular Solar-Powered UAVs in Near Space

ZIRONG LI[1,2], YANPING YANG[1], JUN JIAO[1], AND XIAOPING MA[1]
[1]Institute of Engineering Thermophysics, Chinese Academy of Sciences, Beijing 100190, China
[2]University of Chinese Academy of Sciences, Beijing 100049, China

Corresponding author: Yanping Yang (yangyanping@iet.cn)

This work was supported in part by the National Natural Science Foundation of China under Grant 61901448 and Grant 12002340.

ABSTRACT Maximizing the absorption and utilization of solar energy is a bottleneck issue and hot research concern for high-altitude long-endurance (HALE) solar-powered UAVs (SP-UAVs). This paper investigates the overall design and task optimization for a deformable/reconfigurable SP-UAV platform that utilizes its modular characteristics to optimize the overall solar absorption and structural weight while maximizing its mission utility. First, we establish the energy absorption/consumption model, the aerodynamic model, and the subsystem mass prediction model. Based on these models, the overall parameter design and optimization scheme of a modular SP-UAV is proposed by using heuristic intelligence algorithms. The results show that the loading ratio of the deformable modular SP-UAV increases from 8.2% to 9.8%. Then, the flight processes in both the deformed and the reconfigured cases are verified under task-oriented scenarios. Simulation results indicate that compared with comparable benchmarks with conventional layouts, deformable SP-UAVs are capable of increasing the feasible zone from 72 to 142 days. Additionally, the separation and recombination points are optimized and determined at specific latitudes and dates. A performance analysis shows that separation in the daytime can multiply, thereby increasing the flight range, although the feasible zone shrinks with increasing UAV unit number.

INDEX TERMS Solar-powered UAV, deformable/reconfigurable UAV, radiation absorption, energy utilization optimization, particle swarm optimization.

I. INTRODUCTION

Currently, climate change, energy conservation and emission reductions have become hot and important global issues. To address the future energy shortage crisis, many new energy platforms have been researched and developed, such as new energy automobiles, solar-powered aircraft, and wave power stations. Specifically, the application of SP-UAVs is expected to be an important direction of aircraft development in the future. Conventional fossil-fueled or battery-powered aircraft only support flight for hours or days, while HALE SP-UAVs offer the potential for permanent flight. Compared to low-orbit satellites, the HALE SP-UAV platform has the characteristics of low cost, easy deployment, and flexible operating capability. These advantages have led to the wide use of HALE SP-UAVs in both military and civilian applications, such as for uninterrupted relay communication, high-altitude surveillance, wildfire warning, etc. Currently, representative platforms include Helios (designed by NASA), Zyphyr (designed by Airbus), and Aquila (designed by Facebook Inc.) [1]–[4]. However, most of these platforms are experimental and have not yet been commercialized.

The development of HALE SP-UAVs faces many technical challenges, and the utilization of solar irradiation and the energy density of energy storage batteries are two of the most prominent aspects. Solar irradiation conditions vary based on the season, latitude, time, and flight altitude and are unevenly distributed among the above dimensions, thus causing significant fluctuations in energy absorption. More explicitly, solar energy is not available at night, and SP-UAVs have to store excess energy produced during daylight hours in batteries for night flight. However, the current energy

The associate editor coordinating the review of this manuscript and approving it for publication was Emre Koyuncu.

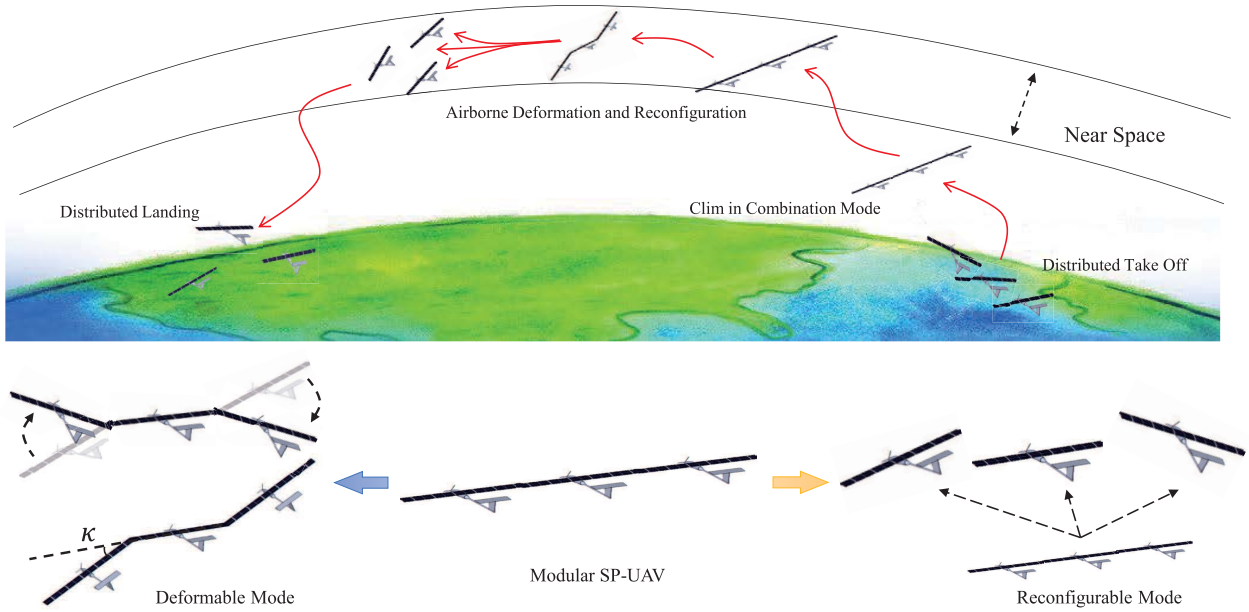

FIGURE 1. Concept for a deformable/reconfigurable SP-UAV.

density of rechargeable energy storage batteries is relatively low, and the ability to provide sufficient energy during the night is a subject of concern. To solve the above problems, researchers are committed to seeking breakthroughs in the overall design, flight control, path planning, and other technologies. Youngblood *et al.* first established a design method for solar-powered aircraft [5]. Then, the subsystems of solar-powered aircraft were modeled and the unique components of solar cells and batteries relative to traditional aircraft were summarized. Noth [6] simplified the solar irradiation environment and subsystem models so that the design process can function analytically. Gao *et al.* in [7] incorporated gravity energy storage into the overall design process to optimize the weight of the battery. Li *et al.* [8] considered a detailed model of the propulsion system and provided an optimized solution for a type of HALE SP-UAV. In terms of path planning, Klesh and Kabamba [9] first mentioned time-based flight attitude control to improve solar absorption and provided an analytical solution of the optimal flight path. These results indicate that SP-UAV capabilities can be enhanced when solar absorption is coupled with aircraft kinematics. Moreover, Wang *et al.* in [10] presents a mission-oriented 3D path planning method that relies on the combination of the Gauss pseudospectral method and ant colony algorithms. However, the scope of application of the above research is limited, and the technical solutions are highly targeted, which lacks practical applicability.

The research and development of SP-UAVs requires interdisciplinary cooperation, and composite schemes that include joint platforms, structures, missions and controls represent a breakthrough direction for future solar UAVs. In terms of solar absorption, a deformable configuration is a promising point for platform design. In 2007, Aurora Flight Sciences Inc. introduced the Odysseus concept, which included a Z-shaped wing configuration and the ability to adjust the dihedral angle of the wing to make the sunlight vertical to the solar cell. Another study [11] proposed a passive method of changing a flying wing into a Z-shaped configuration and back again by utilizing aerodynamic forces and engine thrusts. Wu *et al.* presented an optimal flight planning method [12] and investigated the extra energy harvest of a Z-shaped sun-tracking SP-UAV. Furthermore, the effect of solar cell efficiency, flight latitude and date on optimum wing control, optimum flight attitude planning and energy performance for Z-shaped stratospheric SP-UAVs has been investigated [13]. In addition, N-shaped and Λ-shaped SP-UAV concepts have been presented and the energy benefits have been investigated [14], [15]. Zhu *et al.* [16] regarded Λ-shaped SP-UAVs based on a sun-seeking eternal flight scheme in polar regions.

A reconfigurable concept would provide a potential solution for SP-UAV task utilization. Montalvo and Castello [17] proposed a meta aircraft concept and explored the longitudinal mode of wingtip connected aircraft. The investigation showed that the longitudinal modes of meta aircraft were unaffected. Magill [18] investigated the aerodynamic benefit of wingtip docking UAVs by the wind tunnel test and vortex lattice method, and the results indicated that wingtip docking leads to a 20%-40% increase in performance for hitchhiker aircraft. Based on [17], Wang *et al.* in [19] proposed a mission-oriented energy optimization scheme for a reconfigurable modular SP-UAV on a specific day by

using 3-dimensional path planning optimization. However, the optimization variables of [19] were limited to 24 hours. The above studies indicate that combined platforms and the split-form of SP-UAVs can further improve the task efficiency and essentially increase the utilization efficiency of solar energy.

Based on the above background, we propose that the modular platforms[1] of SP-UAVs should be combined with the optimization of the overall design and mission. The concept of deformable/reconfigurable SP-UAVs is shown in Fig. 1. First, the acquisition of solar energy can be increased through deformation. Second, the mission capability can be improved by effectively utilizing the surplus energy by separating the modular SP-UAV into several sub-UAVs. However, the new constraints introduced by the deformation/reconfiguration concept of the innovative platform cover the overall design, which requires repeated iterations to make the design closed.

Tackling the above technical challenges, the difficulties and contributions of this paper are summarized as follows:

i) The overall design method and process for modular SP-UAVs with innovative configurations are presented. Specifically, the new constraints imposed by deformation/reconstruction are considered.
ii) A joint optimization scheme for energy absorption and utilization is proposed, which essentially converts the energy absorption gain into the mission utility by increasing the degrees of freedom of the SP-UAV structure.
iii) A mass prediction model, solar absorption model, aerodynamic model, and energy consumption model of a deformable SP-UAV are proposed. By combining energy balance and mass balance, a general design approach is proposed to determine the subsystem mass based on the dimension and system parameters.
iv) An optimization framework that combines particle swarm optimization (PSO) and the overall design of a deformable SP-UAV is proposed. Using this design, the total weight of the deformable SP-UAV will be 17.2% less than that of the conventional SP-UAV. Additionally, the feasible number of days for a flight mission can increase from 72 days to 142 days.

The remainder of this paper proceeds as follows. In Section 2, the deformable/reconfigurable SP-UAV is introduced and modeled in detail. Then, in Section 3, the overall design process and the heuristic algorithm are designed. The numerical results of our design and performance analysis are presented in Section 4. In Section 5, the task capability of deformable/reconfigurable SP-UAVs under practical mission scenarios is introduced. Our concluding remarks are provided in Section 6.

II. DEFORMABLE/RECONFIGURABLE SP-UAV MODELING

Fig. 1 shows the proposed deformable/reconfigurable SP-UAV, which features the ability to change its wing shape and the ability to separate into several single units and combine into an integral one. For this innovative platform, we will next present the concept description, solar model, aerodynamic model, mass prediction model, etc.

A. DESCRIPTION OF DEFORMABLE/RECONFIGURABLE SP-UAVs

1) DEFORMABLE SP-UAVs

The main feature of the deformable configuration is that its outer wings can deform upward or downward to adjust the dihedral angle κ against the central wing, with the central wing remaining straight. When solar radiation is present, deformable aircraft adjust their outer wings to seek a vertical position against the solar rays, which means that the energy income is boosted. During energy shortages at night, the deformable aircraft maintains a flat configuration to save energy by increasing the aspect ratio, increasing the lift force, and reducing the induced drag. Note that the feasible range of κ is set to $[-30°, 30°]$, in which the force and moment caused by antisymmetry of the UAV are relatively low, which reduces the compensation by actuators [14].

2) RECONFIGURABLE SP-UAVs

The reconfigurable SP-UAV consists of several independent aircraft by wingtip connection. When the solar intensity is sufficient, reconfigurable aircraft can separate into several subunits, which helps to carry out multiple missions. As shown in Fig. 1, a reconfigurable SP-UAV maintains the combined mode during an energy shortage. When the solar radiation intensity is adequate, it separates to efficiently perform cooperative tasks.

B. FORCE MODELS

1) MASS PREDICTION MODELING

SP-UAV subsystems can be classified into structure, battery, solar cell, maximum power point tracker (MPPT), propulsion, avionics and payload systems. The total mass is the sum of the subsystems:

$$m_{total} = m_{struc} + m_{batt} + m_{sc} + m_{mppt} + m_{prop} + m_{fixed}, \tag{1}$$

where m_{struc}, m_{batt}, m_{sc}, m_{mppt}, m_{prop}, and m_{fixed} denote the mass of the structure, energy storage battery, solar cells, MPPT system, propulsion system, and payload, respectively.

As derived in [6], the mass of subsystems can be estimated in a parametrical way as

$$\begin{cases} m_{struc} = 8.763 N^{0.311} S_{ref}^{0.778} AR^{0.476}/g \\ m_{batt} = k_{batt} Q_{batt} \\ m_{sc} = k_{sc} S_{sc} \\ m_{mppt} = k_{mppt} P_{solarmax} \\ m_{prop} = k_{prop} P_{propmax}, \end{cases} \tag{2}$$

where S_{ref}, S_{sc}, AR, and N represent the reference wing area, solar cell area, aspect ratio and number of boom

[1]Deformable/reconfigurable refers to the characteristics of modular UAVs.

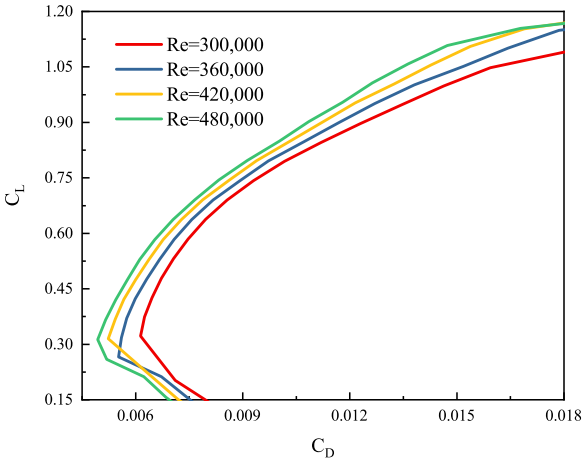

FIGURE 2. AG27 airfoil polar with different Reynolds numbers.

tails, respectively. Q_{batt}, $P_{solarmax}$, $P_{propmax}$ represents the battery capacity, max power of solar energy absorption and max power consumption of propulsion system. g is the gravitational acceleration. k_{batt}, k_{sc}, k_{mppt}, and k_{prop} are the densities of each subsystem. Independent of the other design parameters, the mass of payload m_{fixed} should be a fixed mass, which is defined as a constant value at the beginning of the design process.

2) AERODYNAMIC MODELING

For the deformable/reconfigurable SP-UAV, the key point of the aerodynamic model is to evaluate the effect of configuration changes on lift and drag. The lift coefficient C_L with a low Reynolds number can be calculated by XFoil software, which leads to acceptable accuracy [20].

According to the characteristics of the HALE SP-UAV, the cruise speed is low, which corresponds to a low Reynolds number. In this paper, the AG27 airfoil is chosen to ensure an aerodynamic performance that has a low airspeed and low Reynolds number. The polar of AG27 airfoil is shown in Fig. 2. The drag force consists of profile drag, parasite drag, and induced drag, and the drag coefficient is given by [6].

$$C_D = C_{D0} + C_{Dp} + C_{Di}. \tag{3}$$

The profile drag coefficient C_{D0} is calculated by XFoil software, the parasite drag coefficient C_{Dp} is selected constant because of low Reynolds numbers, and the induced drag coefficient C_{Di} is based on the following equation:

$$C_{Di} = \frac{C_L^2}{\pi eAR}, \tag{4}$$

where e is the Oswald factor. According to [14], the Oswald is selected constant because the simulated aspect ratio is large enough. Note that for a reconfigurable SP-UAV, the induced drag coefficient is affected by the separated or combined mode. When the subunits are linked together, the induced drag coefficient is related to n, the number of subunits [14]:

$$C_{Di} = \frac{C_L^2}{n\pi eAR}. \tag{5}$$

Generally, the lift force of an aircraft can be expressed as

$$L = \frac{1}{2}\rho v^2 S_{ref} C_L, \tag{6}$$

where v is the airspeed, ρ is the air density.

For the deformable SP-UAV, the reference area changes with the dihedral angle. Considering the peculiarity of drag force, profile drag and parasite drag are related to the actual area of the wing while induced drag is related to the reference wing area. Therefore, induced drag also changes with the dihedral angle of the deformable aircraft. Thus, drag force can be expressed as

$$D = \frac{1}{2}\rho v^2 \left[S_{actual}\left(C_{D0} + C_{Dp}\right) + S_{ref}\frac{C_L^2}{\pi eAR} \right]. \tag{7}$$

For conventional fixed wing solar aircraft, S_{ref} and S_{actual} are always identical. However, for deformable SP-UAVs, the values of the two parameters are different because of the nonzero dihedral angle. The reference area S_{ref} varies with the dihedral angle.

3) FORCE BALANCE

As HALE SP-UAVs fly steadily at specific altitudes and speeds, the steady-level flight status is chosen as the design point. When flying at this point, the force balance relationship is relatively concise. The lift force exactly compensates for gravity, and the propeller thrust compensates for the drag force.

$$\begin{cases} L = m_{total} g \\ D = T, \end{cases} \tag{8}$$

where T is the thrust provided by the propulsion system.

C. ENERGY MODELS

1) SOLAR RADIATION RECEIVED MODEL

The Earth coordinate system and the relative position between the solar cell and sun are shown in Fig. 3. $\boldsymbol{n}_s$ is the unit vector whose direction is opposite to the sunlight. α is the solar elevation angle, which refers to the angle between the sunlight and the ground plane. γ is the solar azimuth angle, which refers to the angle between the sunlight and the south. In the earth coordinate system, $\boldsymbol{n}_s$ can be expressed as

$$\begin{cases} \boldsymbol{n}_s = (\cos\alpha\cos\gamma, \cos\alpha\sin\gamma, -\sin\alpha)^T \\ \sin\alpha = \sin\delta\sin\psi + \cos\delta\cos\psi\cos\chi \\ \cos\gamma = (\sin\alpha\sin\psi - \sin\delta)/(\cos\alpha\cos\psi) \\ \delta = 23.45^\circ \sin(360^\circ \dfrac{284 + d_n}{365}) \\ \chi = 15t - 180^\circ, \end{cases} \tag{9}$$

where δ represents the solar declination angle, χ represents the solar time angle, ψ represents the local latitude, and t is

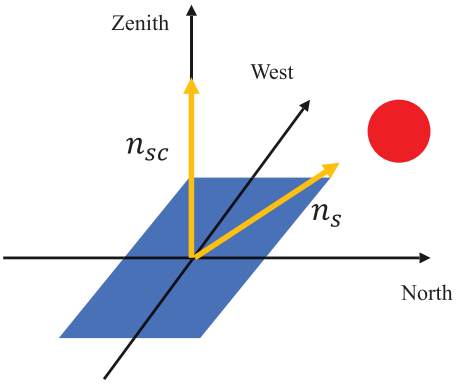

FIGURE 3. Relative position of a solar cell to the sun.

the real sun time. When the real sun time is 12 o'clock, the solar elevation angle reaches a peak. In the earth coordinate system, $\boldsymbol{n}_{sc}$ is the external normal unit vector of the solar cell, as shown in Fig. 3, and it can be determined by the Euler angles of the solar cell as

$$\boldsymbol{n}_{sc} = -\begin{pmatrix} \cos\psi_b \sin\theta_{sc} \cos\phi_{sc} + \sin\psi_b \sin\phi_{sc} \\ \sin\psi_b \sin\theta_{sc} \cos\phi_{sc} - \cos\psi_b \sin\phi_{sc} \\ \cos\theta_{sc} \cos\phi_{sc} \end{pmatrix}, \quad (10)$$

in which ψ_b, θ_{sc} and ϕ_{sc} are the Euler angles of aircraft and solar cells. For the deformable aircraft presented in this paper, θ_{sc} of the central wing and outer wings are 0 and κ, respectively, and ϕ_{sc} is zero because the wing is nonsweepback.

For solar cells, it is generally assumed that only the normal component of solar rays can be absorbed. According to Eq. (9) and Eq. (10), the cosine value of the incident angle of solar rays against the solar cell can be expressed as $\cos\langle \boldsymbol{n}_s, \boldsymbol{n}_{sc}\rangle$. For specific dates, latitudes, altitudes and times, the solar irradiation can be determined by the following equations proposed by Harmats and Weihs [21]:

$$\begin{cases} SI_h = SI_\infty \tau \\ SI_\infty = SI\left\{1 + \varepsilon_0\left[360/365(d_n - 4)\right]\right\}/(1 - \varepsilon_0^2) \\ \tau = 0.5(e^{-0.65AM_h} + e^{-0.095AM_h}) \\ AM_h = AM_0 \cdot p_h/p_0 \\ AM_0 = \sqrt{1229 + (614\sin\alpha)^2} - 614\sin\alpha, \end{cases} \quad (11)$$

where SI_h is the solar intensity, SI_∞ is the solar intensity in outer space, SI represents the mean solar intensity on Earth's elliptical orbital radius. AM_h and AM_0 are the atmospheric quality at local altitude and sea level, respectively. τ is the attenuation factor; d_n is counted from January 1st every year. p_h is the local atmospheric pressure. p_0 is the atmospheric pressure at sea level.

Based on the above derivations, the solar energy converted by solar cells at any time can be expressed as

$$P_{sc} = \sum_i^n \left(\eta_{sc} SI_h cos\left\langle \boldsymbol{n}_s, \boldsymbol{n}_{sc}\right\rangle S\right)_i, \quad (12)$$

where S is the area of solar cells attached to one wing part, η_{sc} denotes the efficiency of the solar cells.

2) ENERGY BALANCE

To achieve perpetual flight, the energy consumption, absorption and storage must be balanced. According to the aerodynamic model and the force balance, the power consumption generated by thrust can be detailed as

$$P_{thrust} = \frac{C_{D0} + C_{Dp} + \frac{C_L^2}{\pi EAR}}{\left[C_L\left(\frac{1+2\cos\kappa}{3}\right)\right]^{1.5}} \sqrt{\frac{2(mg)^3}{\rho S_{ref}}}. \quad (13)$$

It should be noted that the velocity at different flight stages is different because the deformable configuration gives a lift reduction. Considering the efficiency of the propulsion system, the overall power consumption and energy consumption can be calculated by

$$\begin{cases} P_{prop} = P_{thrust}/\eta_{prop} \\ P_{consume} = P_{prop} + P_{fixed} \\ E_{consume} = \int_{24h} P_{consume} dt. \end{cases} \quad (14)$$

Considering the efficiency of the solar cells and MPPT system, the energy input provided by the energy system can be calculated as

$$\begin{cases} P_{absorb} = \eta_{MPPT} P_{sc} \\ E_{absorb} = \int_{24h} P_{absorb} dt. \end{cases} \quad (15)$$

Before dawn and after dusk, the solar elevation angle is low so that the solar power obtained by aircraft is below the power consumed. At that time, the battery provides additional energy. In contrast, between dawn and dusk in the daytime, when the solar power exceeds the total required power, the battery is charged using the extra solar energy obtained by solar cells.

Considering battery charging and discharging, the energy storage of battery E_{chrg} and the energy insufficiency during the night E_{lack} can be calculated by

$$E_{chrg} = \int_{P_{absorb} > P_{consume}} \eta_{chrg}\left(P_{absorb} - P_{consume}\right) dt, \quad (16)$$

and

$$E_{lack} = \int_{P_{absorb} < P_{consume}} \left(P_{consume} - P_{absorb}\right)/\eta_{dchrg} dt, \quad (17)$$

in which η_{charge} represents the charge efficiency from the solar system to the battery and $\eta_{discharge}$ represents the discharge efficiency from the battery to the propulsion system. The constraint of the energy balance can be described by inequalities as

$$\begin{cases} E_{absorb} \geq E_{consume} \\ E_{charge} \geq E_{lack} \\ Q_{batt} \geq E_{lack}. \end{cases} \quad (18)$$

Energy payments and income should be reconciled, the quantity of energy storage must be large enough to cover the

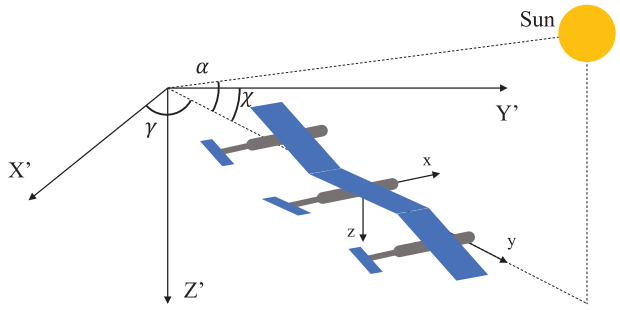

FIGURE 4. Flight strategy of the deformable SP-UAV.

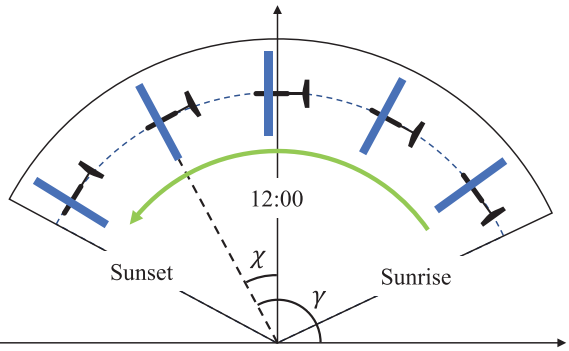

FIGURE 5. Daily yawing angle.

lack at night, and the electric quantity must be larger than the energy insufficiency during the night. According to the mass prediction model, when the relation of equality is satisfied in Eq. (18), the masses of the solar cell and battery have a minimum value.

D. OPTIMIZATION PROBLEM

Based on the characteristics of the modular UAV, we expect to optimize the mission capabilities through an integrated design of overall parameters and flight strategy, as evidenced by an increased load capacity and increased flight range. For the overall design optimization, the goal can be detailed as maximizing the loading ratio under a constant payload, and for the flight strategy optimization, the goal can be detailed as maximizing the mission capability under a fixed mission scenario.

The constraint of this problem can be summarized as follows: (1) The aspect ratio and chord length should be limited in a rational range so that the solution is practical. (2) The weight of subsystems should satisfy the prediction model. (3) The energy absorption generated from the solar model should cover the energy consumption generated from the aerodynamic model in a 24 h cycle. (4) The energy storage of the battery should cover the power consumption when the power absorption is lower than the power consumption.

III. ENERGY-EFFICIENT OVERALL DESIGN OF DEFORMABLE/RECONFIGURABLE SP-UAVs

A. FLIGHT STRATEGY

1) FLIGHT STRATEGY OF DEFORMABLE SP-UAVs

For the deformable configuration, to obtain the maximum solar absorption, the dihedral angle of the outer wing parts must be adjusted according to the orientation of the sun so that the incident angle is minimal and the vertical component of the sunlight vector on the surface of the solar cell is maximal. However, the change in wing shape deteriorates the aerodynamic performance because of the decrease in the reference area, so that at night, the wing remains flat to increase the lift force and reduce the induced drag. The earth surface coordinate frame in the south, east, and down coordinates and the body frame expressed out the nose, out the right wing, and down through the floor are shown in Fig. 4.

During the daytime, to orient outer wings to be exposed mostly to sunlight, the yawing angle and the solar time angle should satisfy

$$\psi - \chi = 90\ deg. \tag{19}$$

Therefore, when the optimal flight direction of the SP-UAV is realized, the sunlight is normal to the axis of the fuselage. As shown in Fig. 5, the optimal trajectory of the deformable SP-UAV is an arc tracking the sun. According to [14], the yawing angle is small enough to be ignored so that steady-level flight is still applicable.

During the daytime, when the sun elevation angle is higher than the maximum dihedral angle, the dihedral angle of the outer wing parts dynamically changes to remain perpendicular to the sunlight, and when the sun elevation angle is lower, the dihedral angle maintains the maximum angle.

$$\kappa = \begin{cases} \kappa_{max}, & \alpha < \kappa_{max} \\ 90deg - \alpha, & \alpha > \kappa_{max}. \end{cases} \tag{20}$$

2) DIHEDRAL ANGLE ANALYSIS OF DEFORMABLE SP-UAVs

As mentioned above, the dihedral angle of a deformable SP-UAV changes adaptively with the solar orientation to obtain a higher efficiency of solar energy absorption. The variation in the dihedral angle is shown in Fig. 6 and Fig. 7. The dates are chosen to coincide with the spring equinox and summer solstice, and the latitudes are 0, 20°N, and 40°N.

a: SPRING EQUINOX DAY ANALYSIS

The alternation point between day and night is at the same time at every latitude. Therefore, the daylight hours are constantly 12 h at every latitude. When the solar elevation angle is low, the dihedral angle of the outer wing part remains at a maximum to compensate for the solar elevation angle as much as possible. At latitudes of 0° or 20°N, the solar elevation angle is higher than 60° at midday and the dihedral angle of the outer wing part can completely compensate for the elevation angle. However, at a latitude of 40°N, the elevation angle is under 60° all day; therefore, the dihedral angle of the outer wing part is maintained at 30° during the day.

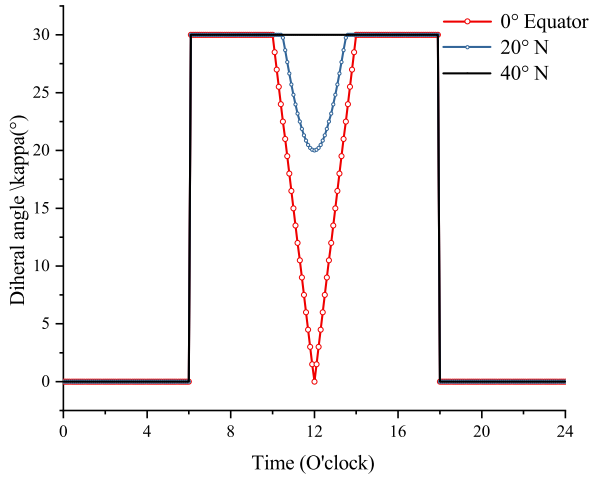

FIGURE 6. Dihedral angle at the spring equinox.

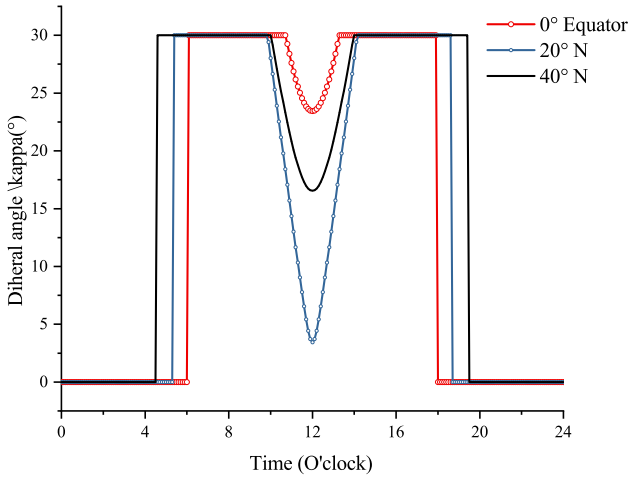

FIGURE 7. Dihedral angle at the summer solstice.

b: SUMMER SOLSTICE DAY ANALYSIS

The daylight hours increase with latitude, with the alternation point occurring earlier. On summer solstice days, the sun is directly over the Tropic of Cancer. Therefore, the minimum dihedral angle appears at 20°N because the elevation angle is closest to 90°. At 0 and 40°N, the solar elevation angle is lower than that at 20°N; therefore, it is compensated by a larger dihedral angle.

3) FLIGHT STRATEGY OF RECONFIGURABLE SP-UAVs

For the reconfigurable form, the aircraft carries out its mission in two modes: the combined mode and the separated mode. The utility is reflected by the total flight distance. During the night, the reconfigurable SP-UAV maintains the combined mode to save energy and boost endurance while the total available energy is restricted by the capacity of the battery. During the day, the M-SPA switches into the separated mode and the subunit is more suitable to perform the mission alone because of the abundance of solar energy.

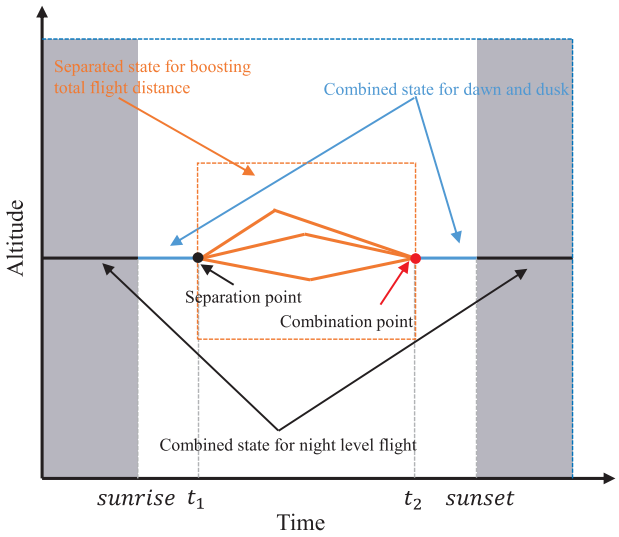

FIGURE 8. Typical flight profile of reconfigurable SP-UAV.

The typical flight profile of a reconfigurable SP-UAV is shown in Fig. 8. The shaded space represents the night. The time that the aircraft switches into separated mode and the subunits switch into combined mode is marked as t_1 and t_2. The separation time is restricted by two factors: real-time energy balance and daily energy balance. The real-time energy balance indicates that at the separation time, the solar energy absorption must be greater than the power consumption. The daily energy balance indicates that over the 24 h cycle, the total energy absorption must be greater than the total power consumption. The two constraints are shown as

$$\begin{cases} P_{consume}(t_1) \leq P_{absorb}(t_1) \\ \int_{24h} P_{consume} dt \leq \int_{24h} P_{absorb} dt. \end{cases} \tag{21}$$

B. OVERALL DESIGN PROCESS

On the basis of the modeling in the previous section, we establish an overall design process. The weight of the subsystems is calculated by numerical iteration, and the core of the overall design method is the energy balance and force balance. There are a series of parameters that should be determined before implementing the general design process. Parameters associated with the physical characteristics of subsystems are named system parameters, such as η_{prop} and k_{solar}, and parameters associated with the performance target are named mission parameters, such as endurance, latitude, altitude, and payload weight. Once the reference area and wing span and other parameters are determined, the structure weight can be determined using Eq. (2).

Taking the overall design solution in [6] as an example, the structure weight accounted for 41.2 percent of the total weight. Using this typical percentage and the structure weight derived from the mass prediction model, we can give an initial estimate of the total weight. From the estimated total weight,

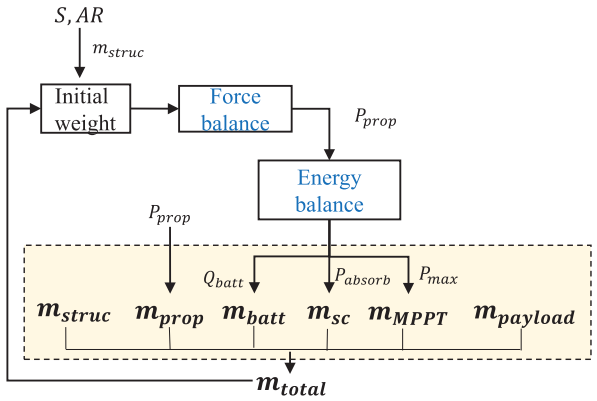

FIGURE 9. Overall parameter selections.

the power consumption of propulsion system P_{thrust} can be determined by Eq. (13); then, m_{prop} is determined. Based on the reference area, the solar area S_{sc} and power absorbed P_{sc} can be calculated from Eq. (12). The weight of MPPT m_{MPPT} and the battery can then be calculated from Eq. (2) and Eq. (18).

As the weight of the subsystems is determined, the total weight of the aircraft can be updated. Then, we can repeat the process above until the calculated total weight and the initial weight converge. The calculation scheme is shown in Fig. 9.

C. HEURISTIC ALGORITHM-BASED PARAMETER OPTIMIZATION

While the mass can be determined by the overall design method mentioned above, a heuristic algorithm is utilized to optimize the geometric parameters for a minimum total mass under specific mission parameter restrictions. Particle swarm optimization simulates the foraging behavior of birds and has clear physical significance [22]. It is efficient in solving continuous solution space optimization problems.

The optimization process requires the following definitions:

Definition 1: Suppose a D-dimensional search space, the swarm consists of n particles $X = (X_1, X_2, \ldots, X_n)$, each particle maintains three vectors, $X_i = (x_1, x_2, \ldots, x_D)$ represents the position in feasible solution space, $V_i = (v_1, v_2, \ldots, v_D)$ represents the velocity of the particle, and $P_i = (p_1, p_2, \ldots, p_D)$ records the best position with an extreme fitness value in history. In addition, vector $P_g = (P_{g1}, P_{g2}, \ldots, P_{gD})$ records the global best position.

First, a series of particles is generated randomly in the feasible solution space, and the fitness values are calculated. During the iteration, particles update the position and velocity according to the two best positions. The calculation formulas are

$$V_i^{k+1} = \omega V_i^k + c_1 r_1 (P_i^k - X_i^k) + c_2 r_2 (P_g^k - X_i^k), \quad (22)$$

and

$$X_i^{k+1} = X_i^k + V_i^{k+1}, \quad (23)$$

TABLE 1. Parameters set for the PSO algorithm.

Parameter	Value
Maximum number of iterations	100
Number of particles	50
Inertness weight factor	0.6
Acceleration factor	2

and

$$P_g^{k+1} = \left\{ X_i^{k+1} | min(f(X_i^{k+1}) \right\}, \quad (24)$$

where ω is the inertness weight, k is the ordinal number of iteration steps, c_1 and c_2 are positive acceleration factors, r_1 and r_2 are random factors in [0,1], and $f(x)$ is the fitness function.

As stated in the previous sections, the loading ratio increases as the total weight decreases. The PSO method is utilized on the overall parameters of the modular SP-UAV. Specific to the overall design of the aircraft, the reference area and aspect ratio are taken as independent design variables. The fitness value is set to be the total weight of the aircraft, which is derived from the iteration of the overall design process. The goal is to minimize the total weight so that the payload ratio is enhanced. As a practical problem, the reference area and aspect ratio in the optimization process should be restricted to a reasonable range [8]. Therefore, the problem can be mathematically stated as

$$\begin{aligned} &min : m_{tot} \\ &s.t. : b_{min} < b < b_{max} \\ &\quad S_{min} < S < S_{max}. \end{aligned} \quad (25)$$

The parameters of the particle swarm algorithm are shown in Table. 1. The optimization framework is shown in Fig. 10.

As a validation, the simulation diagram of the relationship between the fitness and the number of iterations of the PSO algorithm is shown in Fig. 11. It can be obtained from the curve that the fitness converged after 40 iterations, which substantiated that the setting of iteration number is sufficient.

D. ENERGY EFFICIENCY MAXIMIZATION DESIGN

In the actual flight mission, the HALE SP-UAV may fly over a wide time and geographical span. The date, latitude, and longitude changes are not negligible. In this section, we chose an actual mission to evaluate the flight performance promotion of a deformable configuration.

Based on the flight application scenarios of the HALE SP-UAV, the mission simulated in this section includes an aircraft cruising from Urumqi, China$(44°N, 87.4°E)$ to Haikou, China$(20°N, 110.3°E)$, for a distance of 3408 km. The cities are assumed to be points. The distance and direction between cities can be converted to latitude and longitude by Eq. (26), as shown at the bottom of the next page, in which d and ζ are the distance and the direction angle between two cities. *la* and *lon* represent the latitude and longitude.

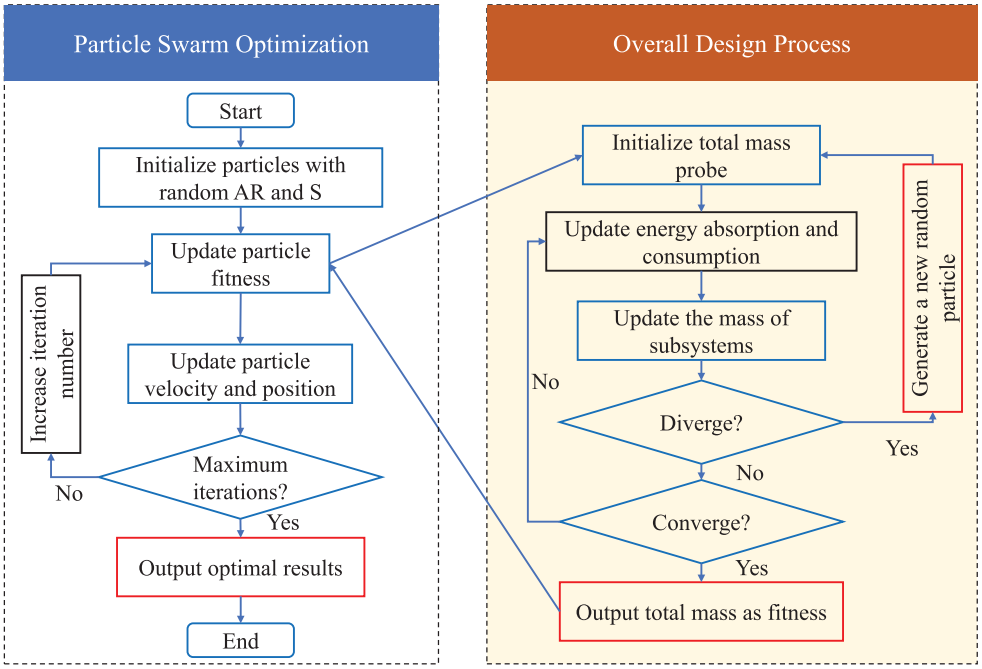

FIGURE 10. Optimization framework.

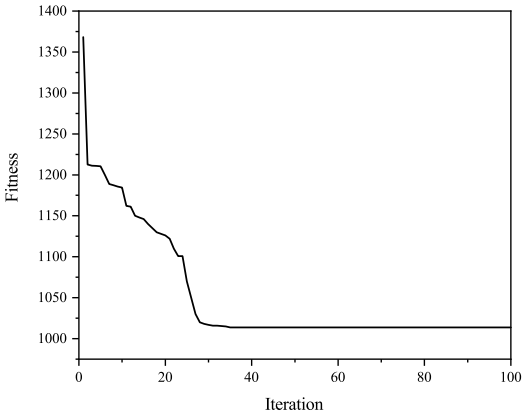

FIGURE 11. Simulation diagram of fitness.

TABLE 2. System parameters settings.

System parameter	Value
$k_{solar}\ (kg/m^2)$	0.4
$k_{batt}\ (Wh/kg)$	240
$k_{prop}\ (kg/kW)$	8
$k_{mppt}\ (kg/kW)$	0.42
η_{sc}	0.3
η_{mppt}	0.97
η_{prop}	0.85
η_{charge}	0.95
$\eta_{discharge}$	0.95
$m_{av}\ (kg)$	50
$P_{av}\ (kW)$	0.2
morphing ratio	2/3
dihedral(°)	0-30

TABLE 3. Mission parameters.

Mission parameter	Value
Flight date	3.22-9.22
Latitude(°)	40
Flight altitude(km)	15
$m_{pld}\ (kg)$	50
$P_{pld}\ (kW)$	1

IV. SIMULATION, VERIFICATION, AND PERFORMANCE ANALYSIS

In this section, we present the numerical results generated by the optimization framework to validate the theoretical analysis. The improved solar aircraft performance associated with deformation is clarified. Before solving the numerical results, the system parameters and task parameters need to be determined first. To ensure the comparability between our scheme and that in previous studies [8], the system parameters and mission parameters are chosen as in Table. 2.

$$\begin{cases} d = 2 * R * \arcsin\left(\sqrt{HaverSin\left(|la1 - la2| + \cos(la1) * \cos(la2) * HaverSin(|lon1 - lon2|)\right)}\right) \\ \zeta = \arctan\left\{((lon2 - lon1) * \cos(la2)) \,/\, (la2 - la1)\right\} \\ HaverSin(\theta) = \sin^2(\theta/2). \end{cases} \tag{26}$$

TABLE 4. General parameter validation.

	Validation case	Results of Li [8]	Error
Total mass(kg)	1224.2	1293	-5.3
Reference area(m^2)	285.2	288	-1.0
Aspect ratio	29.6	28.6	3.49

TABLE 5. Optimal overall design result.

Design variable	Planar	Deformable	Comparison(%)
Total mass(kg)	1224.2	1013.8	-17.2
Reference area(m^2)	285.2	219.1	-23.2
Aspect ratio	29.6	29.6	-

A. OVERALL OPTIMIZATION RESULTS

1) VALIDATION

To validate the optimization method, we choose the common planar wing configuration SP-UAV as the benchmark. The system parameters and mission parameters are chosen to be the same as the reference. The reference area and aspect ratio are taken as independent design variables. The initial value range of the design variables is reference area $100m^2$-$400m^2$ and aspect ratio 10-40. According to reference [8], the daylight hours and solar intensity of the mission start and end days are the same and the minimum solar energy of these days can be obtained in theory. If the energy balance can be achieved in the worst case, the energy balance can be satisfied everywhere; therefore, we selected March 22nd to be the designed date condition.

Under the simulation conditions mentioned above, the optimal general parameters generated by our optimized design frame and those from the reference are shown in the table as follows.

The table indicates that for the planar wing SP-UAV, the relative error of the optimal design results between our method and reference [8] is in an acceptable range, which confirms the validation of our proposed algorithm.

2) COMPARISON WITH THE CONVENTIONAL PLANAR-WING CONFIGURATION

For a comparison, the PSO is used to obtain the design results of a traditional planar wing aircraft. Optimized design variables and results for the two configurations are shown in Table. 5. A comparison between the two configurations shows that the reference area of the deformable configuration is 23.2% less than that of the planar wing while the aspect ratio remains invariant. Although the reduction in the reference area causes obvious lift loss, the lift loss is compensated by the 17.2% reduction in total mass while the payload remains constant.

The mass of the subsystems is shown in Table. 6. Even if the total mass decreases by a significant percentage, the mass of the propulsion system is almost unchanged (only decreases by 1.1%), which means that the maximum power output of the propulsion system remains unchanged because aerodynamic deterioration occurs during daytime hours. The configuration

TABLE 6. Mass of the subsystems.

Subsystem	Planar wing	Morphing wing	Comparison(%)
Structure(kg)	439.1	357.6	-18.6
Battery(kg)	553.2	444.0	-19.7
MPPT(kg)	12.7	9.7	-23.4
Solar cellskg	44.3	28.4	-35.9
Propulsion(kg)	74.9	74.1	-1.1
Fixed mass(kg)	100	100	-

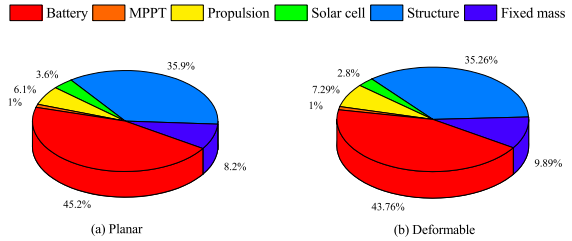

FIGURE 12. Proportion of subsystems.

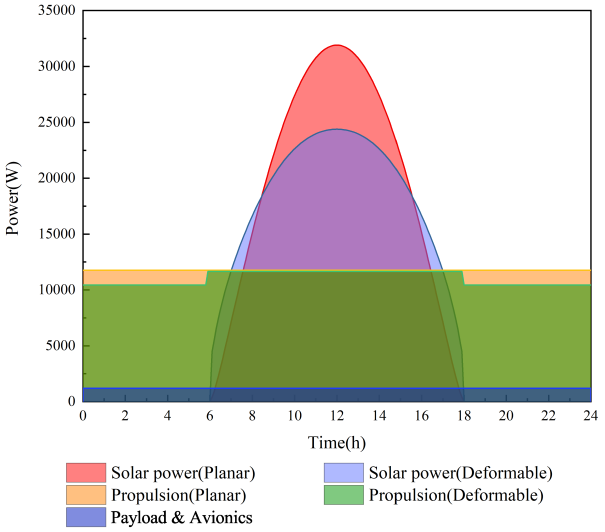

FIGURE 13. Power absorption and consumption of the SP-UAV.

change in the daytime causes a lift decrease and drag increase; thus, the cruise airspeed increases to compensate for the lift loss and the trust increases to balance the drag increase. However, the weight of the structure and battery can be significantly reduced by almost 20%.

Based on the proportion of the subsystems shown in Fig. 12, the proportion of the propulsion system has been enhanced, which means that the sensitivity of the parameters associated with the mass of the subsystem is increased. The proportion of batteries, solar cells, and structures decreases.

The power absorption and consumption with time are shown in Fig. 13. According to Fig. 13, the maximum solar energy absorption decreases significantly because the area of solar cells decreases with the maximum percentage among the subsystems. The power consumption curve of the deformable configuration indicates that the propulsion

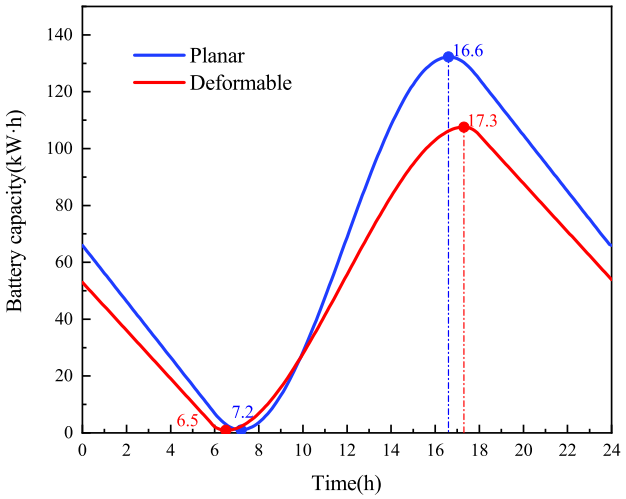

FIGURE 14. State of charge of the battery.

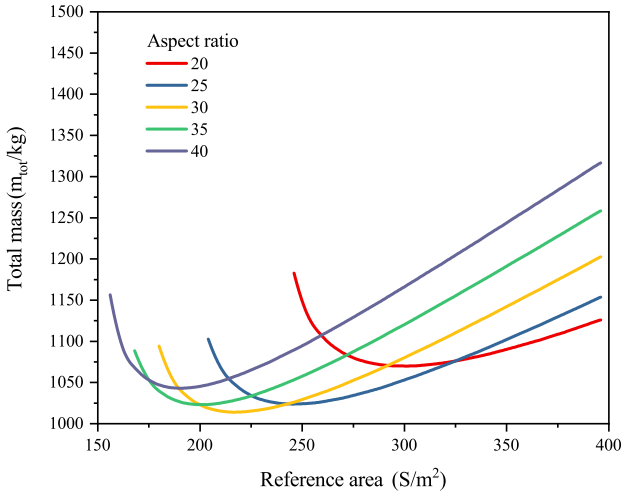

FIGURE 15. Total mass variation of deformable SP-UAV.

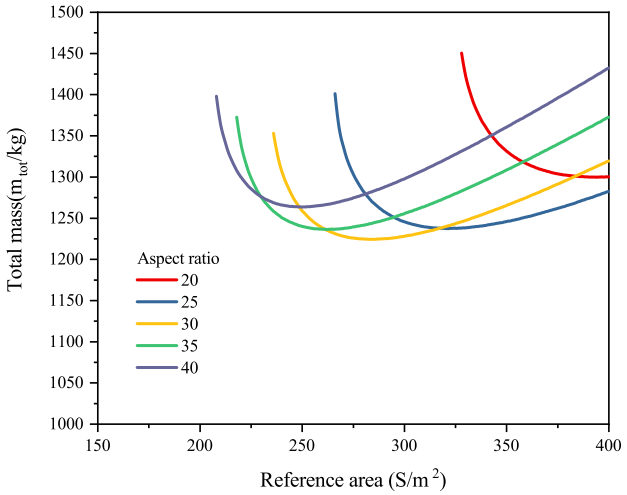

FIGURE 16. Total mass variation of the planar wing SP-UAV.

system actually consumes more energy during daytime hours because of aerodynamic deterioration, as stated by the aerodynamic model. Although daytime deformable SP-UAV consumes more energy than planar SP-UAV, the excess solar energy can compensate for it.

It is noticeable that the absolute value of the slope of the deformable SP-UAV configuration solar absorption curve at dawn and dusk is larger than that of the traditional planar wing configuration. This shape of the curve indicates that the energy conversion efficiency increases at dawn and dusk. Compared to the planar wing configuration, the time when the solar power exceeds the power consumption occurs earlier and the time when the solar power is lower than the power consumption occurs later for the deformable configuration. In other words, the equivalent daytime period is extended for the deformable configuration, which means that the fully solar-supplied duration is longer and the daily running hours of the battery are accordingly shorter, thus causing the energy storage and mass of the battery to decrease.

The electricity storage of the battery is shown in Fig. 14. According to the state of charge curve, the performance promotion of energy utilization can be observed. When the sun rises, the deformable configuration aircraft transforms into an N-shaped aircraft. Because the time of the deformation process is short, it is assumed that the deformation process is a transient process and that the power consumption is also neglected. When the power obtained from the solar panels equals the total power consumption, the energy battery stops outputting electric energy. Then, the power obtained continues to grow, the input power of the propulsion system retains the maximum value, and the surplus power is charged into the battery. As the solar irradiation intensity changes, the slope of the curve increases before noon and decreases after noon. When the power obtained from the solar panels decreases to a lower value than the power consumption, the battery stops charging and reconnects to the propulsion system to provide energy. When the sun sets, the deformable SP-UAV transforms into a planar configuration. According to Fig. 14, the battery capacity of the deformable wing meets the minimum value at 6.5 h and the maximum value at 17.3 h, while those time points of the planar wing are at 7.2 h and 16.6 h, respectively. Comparing the two curves, the first inflection point for the deformable curve, where the battery begins to provide energy, occurs later. In other words, the battery discharge duration of the planar wing SP-UAV (14.6 h) is longer than that of the deformable wing SP-UAV (13.2 h), which indicates that the capacity demand of the deformable configuration at night is less.

B. EFFECTS OF FLIGHT CONDITIONS AND SYSTEM PARAMETERS

The total weight of the two configurations varies with the aspect ratio, and the reference area is shown in Fig. 15 and Fig. 16. According to the figure, the mass-area curve shows that as the reference area increases, the total mass decreases

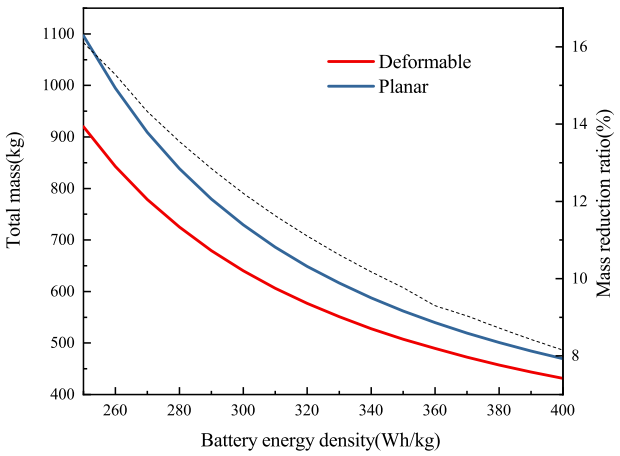

FIGURE 17. Total mass varies with battery energy density.

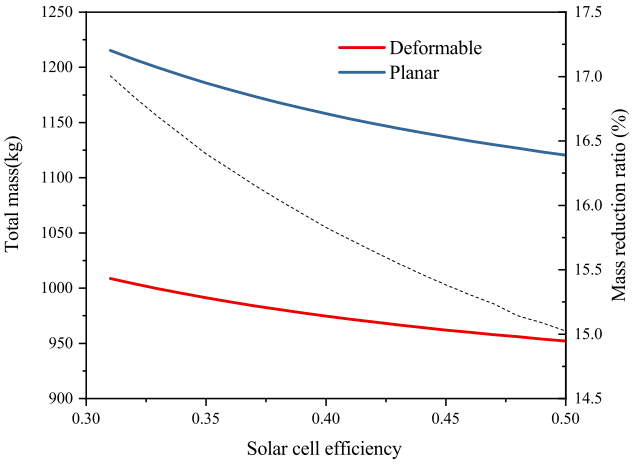

FIGURE 18. Total mass varies with solar cell efficiency.

first and then increases. Both configurations present a lower bound of the reference area in different aspect ratios. The lower bound reaches the minimum when the aspect ratio is near 30 in both configurations, which is identical to the optimization results. The feasible region of the planar wing configuration is narrower than that of the deformable configuration. Given an aspect ratio of 40, the design is feasible when the reference area is below 200 for the planar configuration. When the aspect ratio decreases, the feasible region shrinks obviously because of the increase in the induced drag coefficient and the decrease in the reference area.

Considering the battery energy density as a variable, the optimal SP-UAV mass depending on the energy density is represented in Fig. 17. The energy density of the battery varies from 240 Wh/kg to 400 Wh/kg, the corresponding optimal SP-UAV size obviously declines, and the optimal SP-UAV mass therefore decreases. According to the mass prediction model, as the energy density increases, the mass of the battery decreases for the same battery capacity. As the mass of the battery decreases, the total mass decreases, and the energy requirement therefore decreases, causing the battery mass to decrease further until a new convergence of the total mass is achieved. Therefore, the total weight of the two cases decreases from 1100 kg and 900 kg to 500 kg and 450 kg, respectively.

Using the solar cell efficiency as a variable, the optimal SP-UAV mass based on the solar cell efficiency is shown in Fig. 18. The solar cell efficiency varies from 0.3 to 0.5, and the corresponding optimal SP-UAV total mass decreases slightly. With increasing solar cell efficiency, the solar cell area decreases as the mass prediction model and the mass of solar cells therefore decreases. Although the increase in efficiency improves the quantity of solar energy absorbed during the daytime, the energy balance at night still restricts the mass of the battery; therefore, the total mass, which is mostly contributed by the battery and structure, cannot be reduced significantly.

TABLE 7. Feasible date boundaries.

	Left boundary	Right boundary	Length(days)
Defomable	101(April 11th)	243(September 1st)	142
Planar	135(May 15th)	207(July 25th)	72

C. ANALYSIS OF ENERGY EFFICIENCY MAXIMIZATION

1) ENERGY EFFICIENCY OF DEFORMABLE SP-UAVs

In actual flight missions, SP-UAVs often fly over a wide time range and geographical span. Thus, the date, latitude, and longitude changes are not negligible. In this section, we chose an actual mission to evaluate the flight performance promotion of a deformable configuration.

Based on the flight application scenarios of the HALE UAV, the mission simulated in this section includes an aircraft cruising from Urumqi, China($44°N, 87.4°E$) to Haikou, China($20°N, 110.3°E$), for a straight line distance of 3408 km. The cities are assumed to be points. The distance and direction between cities can be converted to latitude and longitude by Eq. (26), in which d and ζ are the distance and the direction angle between two cities and la and lon represent the latitude and longitude, respectively.

The date when the mission can be completed in the actual mission scenario fluctuates because the flight conditions do not correspond to ideal design conditions. The feasible date boundaries are shown in Table 7.

The deformable SP-UAV can perform tasks over a wider time interval and has greater task adaptability. Taking May 15 as an example, the performance indicators of both during the flight are shown as follows.

The state of charge is shown in Fig. 19. The curve of the deformable SP-UAV is critically above the curve of the common SP-UAV. According to the figure, the deformable SP-UAV allows for faster battery recharge during daylight hours and keeps the battery full longer. While the planar wing exhausts the battery energy at the lowest point of power during the night flight, the deformable wing still has approximately 10% power remaining at the lowest point of power.

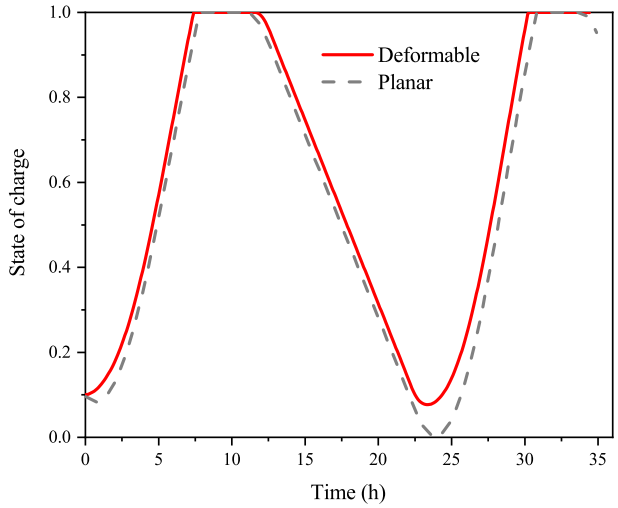

FIGURE 19. SoC for SP-UAV.

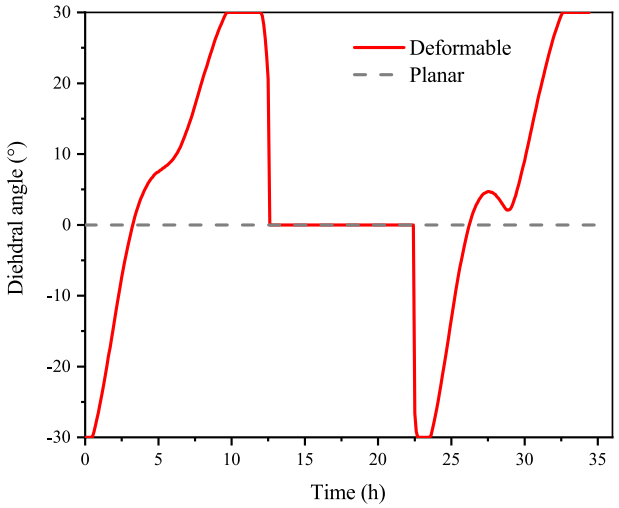

FIGURE 21. Dihedral angle for a SP-UAV.

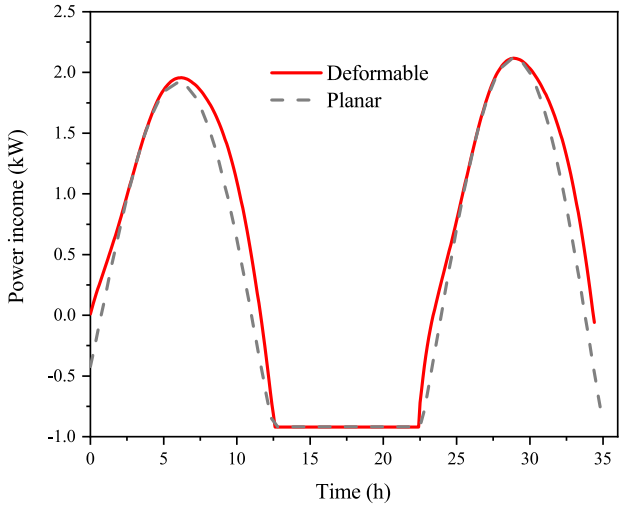

FIGURE 20. Energy income for SP-UAV.

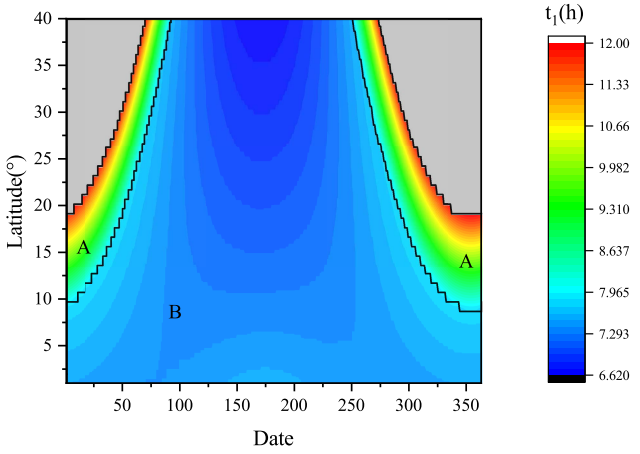

FIGURE 22. Separation time map of the reconfigurable SP-UAV.

The energy income curves during the flight are shown in Fig. 20. We can see from the curves that the energy income of the deformable SP-UAV is higher at all times. The comparison of the two curves shows that the slope of the energy income and expenditure curve is greater in the morning and evening periods for the deformable SP-UAV; thus, the whole energy income reaches a positive value earlier.

For the deformable SP-UAV, the variation of the deflection angle of the outer wing parts with time during the flight is shown in Fig. 21.

2) ENERGY EFFICIENCY OF RECONFIGURABLE SP-UAVs

Considering the solar environment variation during a year, the flight strategy of a reconfigurable SP-UAV differs with the date. While the separated mode presents greater power consumption, the reconfigurable SP-UAV in the separated mode for a longer time and the ability to perform tasks increases as the solar irradiance and the length of daytime increase. The relation between the separation point t_1 and the date and latitude is plotted in Fig. 22 and Fig. 23, and the number of subunits is set to 3 and 5, respectively.

Then, we can discuss the reconfiguration performance according to the figures. Given a specific latitude, as the date approaches the winter solstice, t_1 almost increases. For a specific date, t_1 generally increases with latitude. At low latitudes, the reconfigurable SP-UAV can switch to a separated mode throughout the year, although as the latitude increases, the feasible zone of separation becomes narrow (the gray zone indicates that the reconfigurable SP-UAV cannot separate at that latitude and date). Roughly, when the flight condition is located in the blue zone (marked as B), the separation point is mainly limited by the real-time energy balance, and in the green and red zones (marked as A), the separation point is mainly limited by the daily energy balance. The separation time in zone A is later than that in zone B.

Comparing the two figures, the separation time of 3 subunits s is universally earlier than that of 5 subunits.

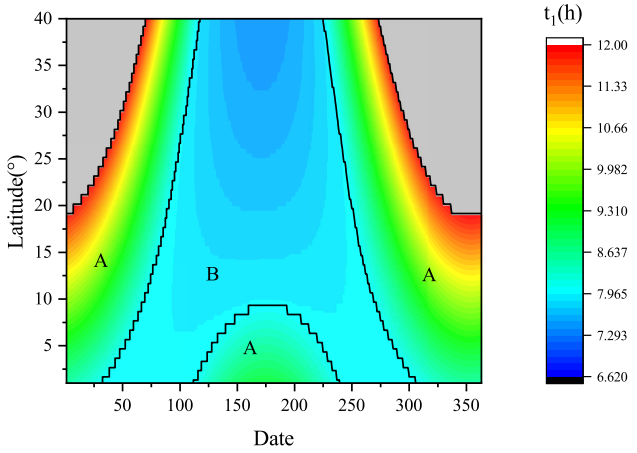

FIGURE 23. Separation time map of the reconfigurable SP-UAV.

With the number of subunits of 5, the control based on the real-time energy balance covers a larger range of dates and latitudes than that of subunits of 3. However, for the two different configurations, the infeasible zones are identical because the feasible zone margin is determined by the integral parameters of the combined mode. On the one hand, the linking mechanism may introduce additional mass. On the other hand, separation and reconfiguration take extra time and energy. As the flight path also restricts the reconfiguration, the short duration of the separated mode may not be technically practicable. Therefore, we define zone B as the technically feasible zone, in which the M-SPA can stably fly a distributed mission. According to Fig. 22 and Fig. 23, as the number of subunits increases to 5, the technically feasible zone shrinks.

V. CONCLUSION

This paper proposed an innovative deformable/reconfigurable SP-UAV platform that can effectively improve the energy absorption and task utility. We focused on the design of the mass model, energy model and flight strategy in the overall design and then proposed an overall design process based on a heuristic algorithm. Through numerical simulation and performance analysis, the following conclusions were obtained: (1) Under certain flight conditions and payloads, the total weight of the deformable SP-UAV is 17.2% less than that of the conventional SP-UAV and continuous flight can still be achieved; (2) During actual flight missions, when the deformable configuration is adopted, the feasible mission days increase from 72 days to 142 days; and (3) With reconfigurable features, the total flight distance increases, although the feasible separation region is negatively correlated with the number of subunits. Future research should investigate the design based on asymmetrical wing parts or subunits or multiple flight profiles.

REFERENCES

[1] X. Zhu, Z. Guo, and Z. Hou, "Solar-powered airplanes: A historical perspective and future challenges," *Prog. Aerosp. Sci.*, vol. 71, pp. 36–53, Nov. 2014.
[2] Y. Hu, Y. Yang, S. Li, and X. Ma, "Computational optimal launching control for ballon-borne solar-powered UAVs in near-space," *Sci. Prog.*, vol. 103, no. 1, pp. 1–19, Sep. 2019.
[3] R. J. Boucher, "Sunrise, the worlds first solar-powered airplane," *J. Aircr.*, vol. 22, pp. 840–846, Oct. 1985.
[4] S. Leutenegger, M. Jabas, and R. Y. Siegwart, "Solar airplane conceptual design and performance estimation," *J. Intell. Robot. Syst.*, vol. 61, nos. 1–4, pp. 545–561, Jan. 2011.
[5] J. Youngblood, T. Talay, and R. Pegg, "Design of long-endurance unmanned airplanes incorporating solar and fuel cell propulsion," in *Proc. 20th Joint Propuls. Conf.*, Cincinnati, OH, USA, 1984, p. 1430.
[6] A. Noth, "Design of solar powered airplanes for continous flight," Ph.D. dissertation, ETH Zurich, Zürich, Switzerland, 2008.
[7] X.-Z. Gao, Z.-X. Hou, Z. Guo, X.-Q. Chen, and X.-Q. Chen, "Joint optimization of battery mass and flight trajectory for high-altitude solar-powered aircraft," *Proc. Inst. Mech. Eng., G, J. Aerosp. Eng.*, vol. 228, no. 13, pp. 2439–2451, 2014.
[8] X. Li, K. Sun, and F. Li, "General optimal design of solar-powered unmanned aerial vehicle for priority considering propulsion system," *Chin. J. Aeronaut.*, vol. 33, no. 8, pp. 2176–2188, Aug. 2020.
[9] A. Klesh and P. Kabamba, "Energy-optimal path planning for solar-powered aircraft in level flight," in *Proc. AIAA Guid., Navigat. Control Conf. Exhib.*, Hilton Head, SC, USA, Aug. 2007, p. 6655.
[10] X. Wang, Y. Yang, D. Wu, Z. Zhang, and X. Ma, "Mission-oriented 3D path planning for high-altitude long-endurance solar-powered UAVs with optimal energy management," *IEEE Access*, vol. 8, pp. 227629–227641, 2020.
[11] P. Mardanpour and D. H. Hodges, "Passive morphing of flying wing aircraft: Z-shaped configuration," *J. Fluids Struct.*, vol. 44, pp. 17–30, Jan. 2014.
[12] M. Wu, T. Xiao, H. Ang, and H. Li, "Optimal flight planning for a Z-Shaped morphing-wing solar-powered unmanned aerial vehicle," *J. Guid., Control, Dyn.*, vol. 41, no. 2, pp. 497–505, Feb. 2018.
[13] M. Wu, Z. Shi, T. Xiao, Z. Chen, and H. Ang, "Effect of solar cell efficiency and flight condition on optimal flight control and energy performance for Z-shaped wing stratospheric solar aircraft," *Acta Astronautica*, vol. 164, pp. 366–375, May 2019.
[14] M. Wu, T. Xiao, H. Ang, and H. Li, "Investigation of a morphing wing solar-powered unmanned aircraft with enlarged flight latitude," *J. Aircr.*, vol. 54, no. 5, pp. 1996–2004, Sep. 2017.
[15] M. Wu, Z. Shi, H. Ang, and T. Xiao, "Theoretical study on energy performance of a stratospheric solar aircraft with optimum Λ-shaped rotatable wing," *Aerosp. Sci. Technol.*, vol. 98, Oct. 2020, Art. no. 105670.
[16] X. Zhu, Z. Hou, J. Zhang, D. Liu, and B. Zhu, "Sun-seeking eternal flight of solar-powered airplane," *J. Aerosp. Eng.*, vol. 27, no. 5, Sep. 2014, Art. no. 06014004.
[17] C. Montalvo and M. Costello, "Meta aircraft flight dynamics," *J. Aircr.*, vol. 52, no. 1, pp. 107–115, Jan. 2015.
[18] S. Magill, "Compound aircraft transport: Wing tip-docking compared to formation flight," Ph.D. Dissertation, Dept. Mech. Aerosp. Eng., Virginia Tech, Chennai, India, 2002.
[19] X. Wang, Y. Yang, D. Wang, and Z. Zhang, "Mission-oriented cooperative 3D path planning for modular solar-powered aircraft with energy optimization," *Chin. J. Aeronaut.*, vol. 35, no. 1, pp. 98–109, Jan. 2022.
[20] M. Drela, *XFOIL User Primer*. Cambridge, MA, USA: Massachusetts Institute of Technology, 2001.
[21] M. Harmats and D. Weihs, "Hybrid-propulsion high-altitude long-endurance remotely piloted vehicle," *J. Aircr.*, vol. 36, no. 2, pp. 321–331, Mar. 1999.
[22] J. Kennedy and R. Eberhart, "Particle swarm optimization," in *Proc. IEEE ICNN*, vol. 4, Nov./Dec. 1995, pp. 1942–1948.

ZIRONG LI received the B.S. degree from Tsinghua University, in 2017. He is currently pursuing the Ph.D. degree in flight vehicle design with the Institute of Engineering Thermophysics, Chinese Academy of Science, Beijing, China. His research interests include the flight vehicle design and solar-powered UAVs. He is currently investigating the project technologies of modular UAV. He also serves as a Reviewer for 2019 IEEE WCSP.

YANPING YANG received the B.S. degree in automation and the M.S. degree in electronics engineering from Xidian University, Xi'an, China, in 2008 and 2013, respectively, and the Ph.D. degree from the National Digital Switching System Engineering and Technological Research and Development Center, Zhengzhou, China, and the Department of Electronic Engineering, Tsinghua University. He is currently a Postdoctoral Researcher with the Institute of Engineering Thermophysics, Chinese Academy of Science, Beijing, China. He has published more than 20 papers around his research directions, including IEEE TRANSACTIONS ON COMMUNICATIONS, IEEE TRANSACTIONS ON VEHICULAR TECHNOLOGY, and IEEE ACCESS. His research interests include UAV formation flight, UAV systems, flight control law design, wireless communications, cognitive radio networks, and network coding. He also serves as a TPC Member for IEEE WCSP 2019 and a Reviewer for the IEEE JOURNAL ON SELECTED AREAS IN COMMUNICATIONS, IEEE TRANSACTIONS ON COMMUNICATIONS, IEEE TRANSACTIONS ON VEHICULAR TECHNOLOGY, ICC, and IEEE GLOBECOM.

JUN JIAO received the M.S. and Ph.D. degrees from Northwestern Polytechnical University. His research interests include deformable propeller design, flight vehicle design, and solar-powered UAVs. He has published more than ten papers around his research directions and has undertaken solar-powered UAV projects, the National Natural Science Foundation of China and China Postdoctoral Fund.

XIAOPING MA received the bachelor's, master's, and doctor's degrees in aircraft design from Northwestern Polytechnical University, in 1983, 1988, and 2008, respectively. He has been engaged in the research and development of UAV for a long time and has participated in various types of UAV, where he is serving as the Deputy Chief Engineer and a Chief Engineer. He has published more than 20 papers that related to UAV design, among which five were retrieved by EI/SCI/ISTP/SSCI. His research interests include the UAV systems, the aircraft and structure design, launching and recovering technique, and system flight test. He also serves as a Senior Member for the Aviation Society of China. He has won the First Prize and the Second Prize of National Science and Technology Progress, the Second Prize of National Commission of Science, Technology and Industry for National Defense, and the First Prize and the Second Prize of Ministerial Award.